ELSEVIER

Catalysis Today 81 (2003) 247–262

CATALYSIS TODAY

www.elsevier.com/locate/cattod

# Recent developments in the selective oxidation of propane to acrylic and acetic acids

J.C. Védrine*, E.K. Novakova, E.G. Derouane

*Department of Chemistry, The Leverhulme Centre for Innovative Catalysis, The University of Liverpool, Oxford Street, Liverpool L69 7ZD, UK*

**Abstract**

The oxidation of propane to acrylic and acetic acids has been studied using a $Mo_1Nb_{0.08}Sb_{0.25}V_{0.3}$ mixed oxide catalyst, calcined and activated before reaction under different conditions ($T = 500$ or 600 °C in atmospheres of $N_2$, static air, and flowing air (dry or with water or ammonia addition)). Catalytic testing was performed at 400 °C in a plug flow microreactor and the characterisation of the catalysts was carried out by XRD, XPS, BET, FT-IR and ammonia TPD. The best conditions for acrylic acid (AA) formation are calcination at 500 °C under $N_2$, followed by activation at 500 °C prior to reaction under helium. The selectivity to acetic acid was found to be rather high, which was assigned to the presence of Sb instead of Te, which is used most often. The presence of all four elements, Mo, Nb, Sb and V, was found necessary to achieve high selectivities in acrylic and acetic acids. The presence of several crystalline phases, such as $Sb_4M_{10}O_{31}/Sb_2M_{10}O_{31}$ with M: Mo (major), Nb and/or V (minor), $SbVO_4$, sub-oxides of $MoO_3$, such as $Mo_8O_{23}$ and $(M_xM_yMo_{1-x-y})_5O_{14}$ with $x$ and $y$ referring to low amounts of V and Nb, and some amorphous phases, such as $Sb_2O_4$, was shown to be important in order to orientate the reaction toward the production of acrylic and/or acetic acids. The presence of $MoO_3$ in all air-calcined samples was found to be detrimental to the selective oxidation of propane.

This work exemplifies further the general concept of multicomponent oxide catalysis for heterogeneous selective oxidation, which involves low acidity, a synergistic effect between several solid phases and the role of shear/defective and even XRD amorphous, structures facilitating the redox mechanism of the reaction.


*Keywords:* Propane selective oxidation; Acrylic & acetic acids; Redox vs. acid–base; MoNbSbVO mixed oxides; $(M_xMo_{1-x})_5O_{14}$ sub-oxide with M = V or Nb; Activation conditions

## 1. Introduction

The selective oxidation of light alkanes ($C_1$–$C_5$) to form the corresponding olefins, alcohols, aldehydes, anhydrides or acids has been largely studied in the past 20 years for two main reasons. The first one is economical since alkanes are much cheaper and more abundant than the corresponding olefins. The second one is fundamental since the way by which the alkane is activated and functionalised into an oxygenate remains unclear and challenging.

There are two main actors in an oxidation reaction: the reactants (the hydrocarbon and the oxygen species) and the catalyst. In short, one needs:

1. to *activate* both the oxygen and the hydrocarbon, and more specifically to determine the role of the adsorbed/lattice oxygen species and the importance of the mode of hydrocarbon adsorption;

* Corresponding author. Present address: ENSCP, Laboratoire de Physico-Chimie des Surfaces, 11 Rue P. & M. Curie, Paris F-75005, France. Tel.: +33-14633-5587; fax: +33-14634-0753.
*E-mail addresses:* vedrine@liv.ac.uk, jacques-vedrine@enscp.jussieu.fr (J.C. Védrine).

0920-5861/03/$ – see front matter © 2003 Elsevier Science B.V. All rights reserved.
doi:10.1016/S0920-5861(03)00125-1

2. to *ensure* the reactivity of the reactants and, more importantly for selective oxidation, to control the reactivity of the primary and secondary products to avoid further oxidation to $CO_x$;
3. to *control* the mechanism of the hydrocarbon transformation (heterolytic versus homolytic C–H bond activation), the desorption rate of reaction intermediates, and the contribution of homogeneous reactions, especially when the temperature exceeds 400 °C;
4. to *tune* the surface properties of the solid catalyst to match several reaction requirements, comprising H atom(s) abstraction, oxygen atom(s) insertion and electron transfers.

In this paper, a single example is discussed, namely the direct oxidation of propane to acrylic and acetic acids on Mo/Nb/Sb/V mixed oxides, as described in Mitshubishi, Toa Gosei, and Rohm & Haas patents and synthesised using a slurry method, followed by calcination and activation in different conditions [1–4]. A study of the kinetic and reaction mechanism of both propane and propene oxidations to acrylic and acetic acids, and catalysts characterisation before and after catalytic testing, have allowed [5,6] the description of such catalysts and of their behaviour during catalytic reaction. A combinatorial approach to the preparation of this mixed oxide system, either as bulk or supported on silica beads, as well as its testing using high throughput experimentation has also been carried out and will be published elsewhere [7].

## 2. General features of selective oxidation reaction on metal oxide catalysts

Many factors play a role in selective oxidation reactions on metal oxide catalysts and the complexity of such catalysts is widely recognised [8]. It is usually accepted that:

(a) Selective oxidation reactions in heterogeneous catalysis with oxides proceed through a Mars and van Krevelen redox mechanism [9]. In such mechanism, the active site oxidises the reactant molecule R creating a lattice oxygen $O_L$ vacancy □, and being reduced yields the product P. The catalyst is then re-oxidised by gas phase oxygen in a subsequent step, according to the following scheme, where $p$ represents the partial pressure and $\theta$ the surface coverage by the hydrocarbon:

$$R_{(g)} + O_L \xrightarrow{k_{red}} P + \square \text{ and } \square + \tfrac{1}{2}O_2 \xrightarrow{k_{ox}} O_L$$

with $r_{red} = k_{red} p_R \theta$ and $r_{ox} = k_{ox} p_{O_2}^n (1-\theta)$

(b) The reaction proceeds entirely at a single site, consisting of a cluster/ensemble of atoms. This concept has been first proposed by Haber and co-workers [10,11], and was confirmed in many cases, e.g. for bismuth molybdate catalysts by Grasselli and Burrington [12] in the (amm)oxidation of propene to (acrylonitrile) acrolein, and extended to many other mixed oxides [13,14]. The reaction is usually schematised as a sequence of consecutive steps. The first step, H atom extraction from the hydrocarbon, is followed by the formation of an adsorbed complex to which lattice oxygen atom is added, etc.

(c) The rate-determining step (rds), controlling the overall rate of the reaction, is usually the first H-abstraction from the hydrocarbon. Other steps, such as further H atom extraction and product desorption, are usually significantly faster.

Selective oxidation reaction involves one or several H atom(s) abstraction from the hydrocarbon molecule, one or several O atom(s) insertion from the lattice and several electrons transfer. For instance, for the *n*-butane oxidation to maleic anhydride, eight H atoms are extracted from *n*-butane molecule, three O atoms are incorporated and there are six electrons transferred according to:

$$C_4H_{10} + 7O^{2-} \rightarrow C_4H_2O_3 + 4H_2O + 6e^-$$

This means that surface cations are reduced and dehydroxylation occurs creating lattice oxygen vacancies, which are further replenished by molecular oxygen that re-oxidises the cations by electron transfer at the surface or within the solid. This implies the existence of collective properties at the solid surface, in particular lattice oxygen mobility and electron conductivity [15,16]. This means that, even if the concept of localised active sites holds true, collective properties of the solid also take part in the catalytic act [17,18].

In general, the oxygen requirement of the selective reactions is less demanding than that of the

non-selective reactions. It follows that restricting the availability of lattice oxygen anions at and around the active site should favour the selective oxidation reactions over the total oxidation reactions. This was clearly demonstrated by Grasselli and co-workers [19,20] for $USb_3O_{10}$ used as catalyst for the propene oxidation to acrolein. An important feature is the dilution of the ions (U) responsible of the redox activity within the active site, brought about by the presence of Sb, which does not readily change its oxidation state. The dilution is a consequence of the crystallographic plane cleavage, on which the active site is located. This is the site isolation principle introduced by Callahan and Grasselli [21] and reviewed recently [22].

Multicomponent metal oxide catalysts are known since the early seventies, following the pioneering works by Sohio Researchers [12,19–21], to be the most efficient for the selective oxidation and ammoxidation of hydrocarbons and organic oxygenates. Different hypotheses have been proposed to explain the enhancement in both catalytic activity and selectivity. These include morphology changes under catalytic conditions [23], interaction between phases [24], contamination/wetting of one phase by the other under catalytic conditions [25] or remote control (oxygen spill-over) process [26,27]. The latter concept was supported recently [28] for acrolein oxidation to acrylic acid (AA) when antimonates, considered to be oxygen donors, were added to a Mo, V, W and Cu mixed oxide catalyst.

### 2.1. Acid–base features of metal oxides [18]

Oxygen has a highly electronegative character and its bond with a metal is ionic, while it is covalent with a non-metal. Oxides of metals at high oxidation state, such as $V^{5+}$ or $Mo^{6+}$ are characterised by a covalent metal to oxygen bond and behave as acidic oxides, whereas the same elements at lower oxidation state have more ionic character and behave as basic oxides. The acid–base characteristics of the oxide have a major effect on the activation of the reactants, the relative rates of competitive reaction pathways, and the rate of adsorption and desorption of the reactants and products. These characteristics may change under reaction conditions depending on the oxidation state of the catalyst surface.

On a basic oxide, one expects the allylic species, formed by the first H abstraction, to be anionic, and π-bonded to a Lewis acid site. It is then susceptible to an attack at the α-hydrogen by neighbouring lattice oxygen. The allyl species can be side-on or end-on bonded depending on the metal. The former may undergo nucleophilic attack and give a ketone or an aldehyde, while the latter may dimerise.

On an acidic oxide, the allylic species exist as carbocations giving an unsaturated ketone R–CO–CH=$CH_2$ or aldehyde R–CH=CH–CHO. Another possibility is that the hydrocarbon is attacked by a Brønsted acid site and forms an alkoxide intermediate, which gives a saturated ketone R–CO–$CH_2$–$CH_3$. It is clear that controlling the acid–base properties of a catalyst surface will affect the first C–H activation and first reaction intermediate, and thus, the overall reaction scheme.

### 2.2. Nature of the oxygen species and structural/crystallisation state changes during catalytic reaction

Various types of surface oxygen species, such as $O_{2ads}$, $O_{ads}$, $O_3^-$, $O_2^-$, $O^-$, $O^\bullet$, lattice $O^{2-}$ anions, etc. may exist and are usually classified, following Bielanski and Haber's suggestions [29,30], as electrophilic/nucleophilic. The electrophilic oxygen is generally considered as non-selective at variance with nucleophilic and thus more basic oxygen, such as lattice $O^{2-}$ anions.

Transition metal oxides, which constitute the major family of catalysts for selective heterogeneous oxidation, are non-stoichiometric compounds whose compositions depend on the surrounding gas phase environment. The formation of point defects or alteration of the linkage between polyhedra under catalytic reaction conditions, as a result of lattice oxygen incorporation in the adsorbed hydrocarbon (Mars and van Krevelen mechanism) leads to the reorganisation of the surface and to the formation of extended defects in crystallographic shear planes. This has been demonstrated by Gai [31] for VPO catalysts during *n*-butane oxidation to maleic anhydride. It follows that the oxide surface is changing during catalytic reaction and can be considered as "living and in breathing movement". It also corresponds to the frequent suggestion that the catalyst uppermost surface is rather labile, and even amorphous [32,33]. The present paper will also emphasise the role of these structural features and changes.

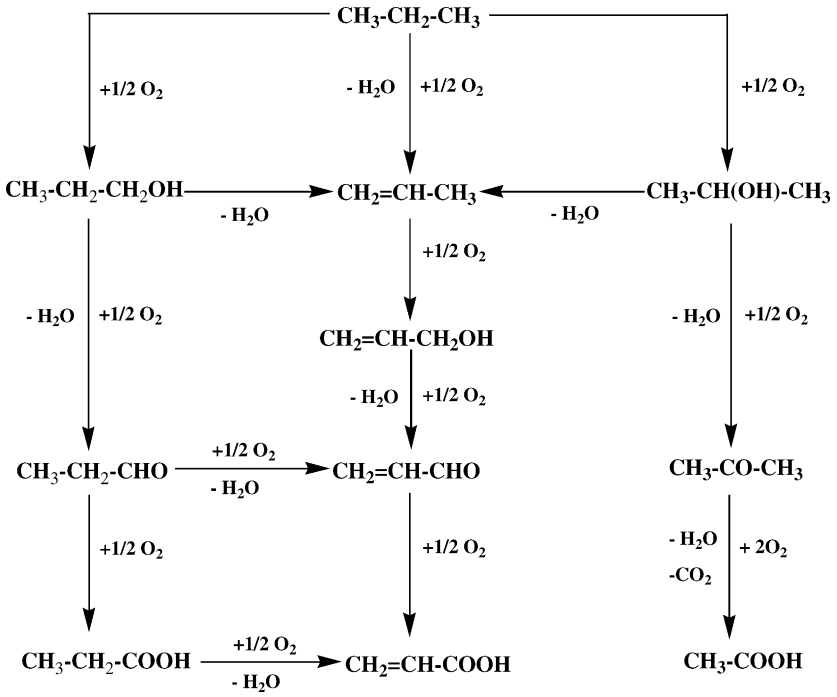


Fig. 1. Main oxygenated products of partial oxidation of propane from [36].

## 3. Propane oxidation to acrylic and acetic acids on MoNbSbV mixed oxides

The synthesis of MoNbV(Sb)Te mixed oxides and their catalytic properties for propane (amm)oxidation have already been largely studied in industry and academia. The reaction mechanism has also been discussed in the literature [18,34–38] and is summarised in Fig. 1. In a previous study [5,6], we have shown that propene is the major primary product, which is further transformed to acrylic acid. By studying propene oxidation at the same temperature, we observed that acrolein is the major primary product and acrylic acid, a major secondary product. The other primary product, acetone, yields acetic acid as a secondary product in an alternative pathway. We have also shown that calcining the precursor in nitrogen at 500 or 600 °C and activating the catalyst in helium at 500 °C favour the main pathway via propene and the acrylic acid formation. When calcination and activation were performed in air, the second pathway via acetone giving acetic acid and $CO_x$ was favoured. It appeared therefore important to investigate further the influence of calcination and activation atmospheres, and temperatures, on catalytic performance and to relate the latter to structural changes of the catalyst.

### 3.1. Experimental part

A $Mo_1Nb_{0.08}Sb_{0.25}V_{0.3}O_n$ mixed oxide sample was prepared using the slurry method described in the patent literature [4], followed by drying the solid at 120 °C and calcining it for 2 h. Calcination conditions and further activation in air or nitrogen and the temperature were reported previously to be important parameters controlling catalytic performance, mainly for the acrylic acid yield [5,6]. The former studies have been extended by calcining the sample at 500 or 600 °C under different atmospheres: nitrogen, ammonia + air, humid air, dry air, static or flowing air. The catalyst was further activated at 500 °C under oxidative (20% $O_2$ in He) or inert (He) atmospheres for 1 h before starting the reaction. Catalytic experiments were performed at 400 °C in a continuous flow fixed bed micro-reactor using 500 mg catalyst diluted in SiC to a total volume of 1.2 $cm^3$ and a flow rate

of 30 $cm^3\,min^{-1}$, GHSV = 1500 $h^{-1}$. The feed composition was propane, oxygen and water in the ratio 52/13/35 vol.%. The condensable products (acrylic and acetic acids, acrolein, acetone, water, etc.) were collected for 1.5 h in a system of two successive traps at room temperature and the gases were analysed on-line (propane, propene, carbon oxides, ...). The catalytic results were calculated by integrating the data for gases for 1.5 h and adding those to the liquid condensate data, assuming a 100% C balance.

The catalysts were characterised using BET, XRD, FT-IR, XPS and $NH_3$–TPD techniques. The surface area measurements were performed with a Micromeritics ASAP2000 apparatus using nitrogen as probe. The XRD characterisation was carried out at room temperature using a D-5000 Siemens diffractometer with a Co anticathode. The IR spectra were recorded at ambient temperature, as KBr self-supported disks (KBr/catalyst = 400/1). XPS analyses were performed using a VG Scientific spectrometer with Mg anode as a source of non-monochromatised X-ray radiation. All binding energy values were determined by using the $C_{1s}$ line as a reference at 284.5 eV. The $NH_3$–TPD characterisation was carried out with a Micromeritics TPO/TPR 2900 apparatus in the temperature range 200–600 °C under He flow after saturation of the sample with pure ammonia (50 $cm^3\,min^{-1}$) at 80 °C. For quantitative determination of the desorbed $NH_3$, a calibration of the detector signal was done by performing a TPD in He up to 800 °C on three $NH_4$-exchanged MFI zeolites with different Si/Al ratio and the amount of the desorbed ammonia was plotted versus the calculated concentration of ammonia for a given weight of zeolite. The acid–base titration of the catalysts was done against a standardised solution of $NH_4OH$ (0.1014 N) using 1:1 mixture of methylene blue and neutral red (colour change at pH = 7) for an indicator. The elemental composition of the samples was determined either by atomic absorption at UMIST, Manchester, UK, or by ICP (CIROS 120 SOP from Spectro) techniques.

### 3.2. Effect of calcination environment on phase formation

The XRD patterns of the catalyst calcined in different conditions are given in Fig. 2. It is seen that moving from an oxidative to an inert atmosphere, the nature of the catalyst phases changes significantly. The identification of the phases present after calcination under air or nitrogen and before and after activation at 500 °C under $N_2$ or under 20% $O_2$ in He prior to catalytic testing, are summarised in Table 1(A); before reaction. It appears that after calcination under nitrogen,

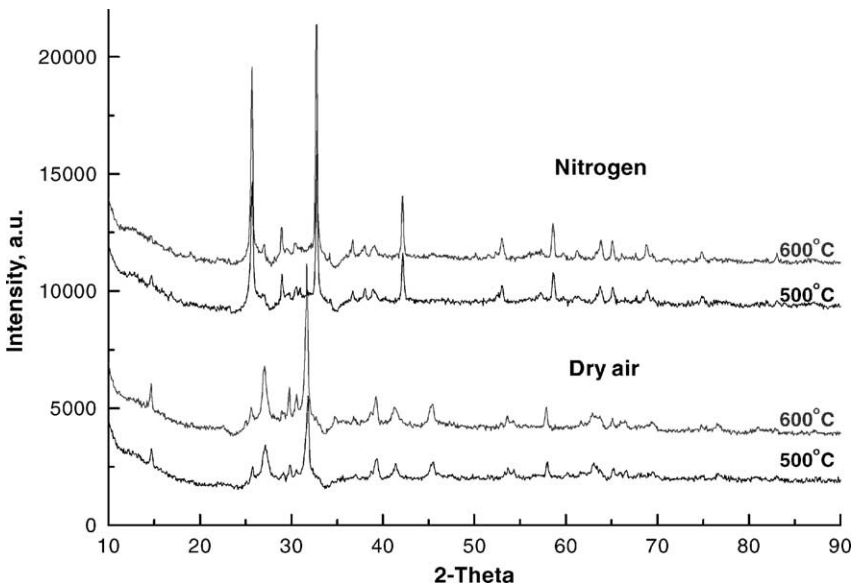


Fig. 2. XRD patterns of $N_2$- and air-calcined catalysts at 500 and 600 °C, using Co Kα radiation.

Table 1
Phases detected by XRD (Co source) for both air and nitrogen calcined samples at 500 or 600 °C and activated under $N_2$/He or $O_2$/He at 500 °C

| | XRD phases | | | | | |
|---|---|---|---|---|---|---|
| | $MoO_3$ (35–0609) | $Mo_8O_{23}$ (05–0339) | $VSbO_4$ (35–1485) | $Sb_4Mo_{10}O_{31}$ (33–0104) | $Sb_2Mo_{10}O_{31}$ (33–0105) | M–Mo–O[a] (M: Nb and V) |
| (A) before reaction | | | | | | |
| Calcination atmosphere | 14.9; 27.1; 29.0; 31.5; 39.4[b] | 25.5; 29.8; 30.3; 34.6; 38.6; 54.9[b] | 31.9; 40.9; 45.7; 63.1; 66.7[b] | 25.7, 33.1; 42.2; 58.5[b] | 25.6; 30.7; 31.2; 35.7; 40.7; 57.3[b] | 25.7; 27.1; 28.8; 30.4; 36.8; 39.1[b] |
| 500 °C air prior/after activation in $O_2$/He | Very strong | Weak | Medium | – | – | Strong |
| 600 °C air prior/after activation in $O_2$/He | Very strong | Weak | Medium | – | – | Strong |
| 500 °C $N_2$ prior/after activation in He | – | Weak | – | Very strong | – | Strong |
| 600 °C $N_2$ prior/after activation in He | – | Weak | – | Very strong | – | Strong |
| 500 °C $N_2$, activation in $O_2$/He | – | Weak | – | – | Very strong | Strong |
| 600 °C $N_2$, activation in $O_2$/He | – | Weak | – | Strong | Strong | Strong |
| (B) after 4.5 h reaction | | | | | | |
| 500 °C $N_2$, activation in $O_2$/He | – | Weak | – | Weak | Very strong | Strong |
| 600 °C $N_2$, activation in $O_2$/He | – | Weak | – | Very strong | Medium | Strong |

The numbers in parentheses refer to JCPDS files.
[a] M–Mo–O corresponds to $(M_xMo_{1-x})_5O_{14}$ with M: V and/or Nb.
[b] Main $2\theta$ values (°).

$Sb_4Mo_{10}O_{31}$ and to a lesser extent $(M_xMo_{1-x})_5O_{14}$ with M: V and/or Nb are the major phases with traces of $Mo_8O_{23}$, while after calcination under oxidative atmosphere, the major phases are $MoO_3$, $VSbO_4$ and $(M_xMo_{1-x})_5O_{14}$ with traces of $Mo_8O_{23}$. Moreover when the $N_2$ calcined samples were activated before reaction under 20% $O_2$ in He, $Sb_4Mo_{10}O_{31}$ (which can be written as $Sb_4^{3+}Mo_{10}^{5+}O_{31}$) disappeared for the 500 °C calcined sample and decreased in intensity for the 600 °C calcined sample while the $Sb_2Mo_{10}O_{31}$ (which can be written as $Sb_2^{5+}Mo_8^{5+}Mo_2^{6+}O_{31}$ or $Sb_2^{3+}Mo_{10}^{5.6+}O_{31}$) phase was formed (see two bottom rows in Table 1(A); before reaction). No change was noticed for activation under He.

The catalysts calcined in static air (grey colour) or in air flow (green colour), with or without addition of $NH_3$ or $H_2O$, are only slightly different by their physical appearance (colour), their surface area and their crystallite size. Their XRD patterns are shown in Fig. 3. It may be noted that the sample calcined in static air shows specific peaks at $2\theta^\circ$ near 14.2, 19, 26, 29, 36.5, 38 and 39 ($d$ = 7.24; 5.42; 3.98; 3.57; 2.86; 2.75 and 2.68 Å) with respect to the $N_2$ or air-calcined samples. The peak assignment is quite difficult because of peak overlap due to the presence of several different phases. Nevertheless, it is suggested that the latter peaks belong to the $(M_xMo_{1-x})_5O_{14}$ phase. If our interpretation is correct, we can conclude that $MoO_3$ phase is present in appreciable amounts for all air calcined samples, but not for static air and $N_2$-calcined samples, while the $(M_xMo_{1-x})_5O_{14}$ phase, seen mainly by the $2\theta$ peaks near 19, 29 and 36.5, is present for all samples in the decreasing order: static air > $N_2$ > $H_2O$/air > $NH_3$/air ∼ dry air.

In parallel with the phase identification by XRD, FT-IR measurements on the differently calcined samples were also performed in order to obtain additional information about the crystalline phases. All characteristic bands are in the region of skeletal vibrations (1100–400 $cm^{-1}$), which makes their interpretation extremely difficult (Fig. 4). There is limited literature data on the position of IR bands in Mo, V, Sb and Nb binary or ternary mixed oxides, which as shown by XRD, are the main phases formed during calcination. The interpretation is further complicated by the shifts in peak position of the mixed oxides in comparison to the corresponding single oxides.

Fig. 4 shows that the catalysts calcined in oxidative atmosphere have similar FT-IR spectra with three very strong bands. The band at 990 $cm^{-1}$ is characteristic for $\nu(Mo^{6+}{=}O)$ vibration in $MoO_3$ together with a weak band at 818 $cm^{-1}$. The bands at 870–883

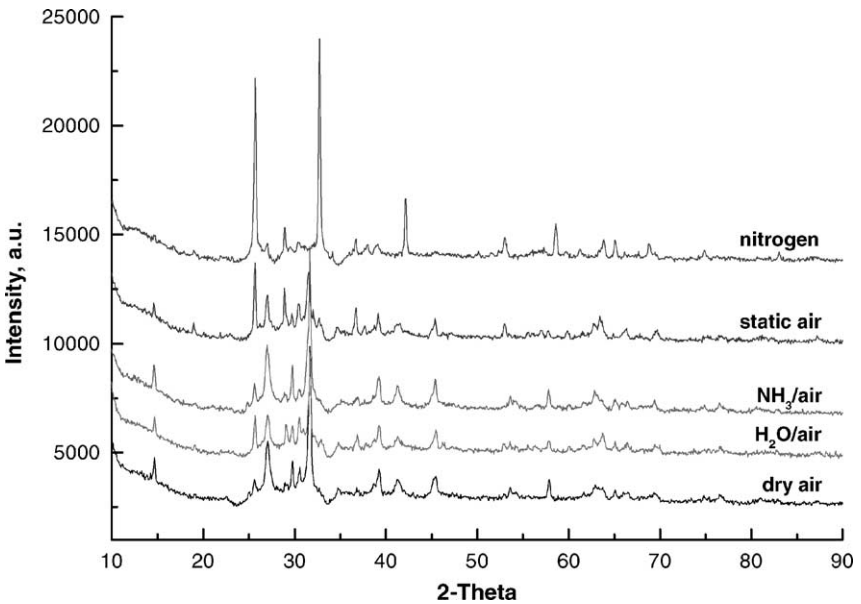


Fig. 3. XRD patterns of all catalysts calcined at 600 °C under various atmospheres, using Co Kα radiation.

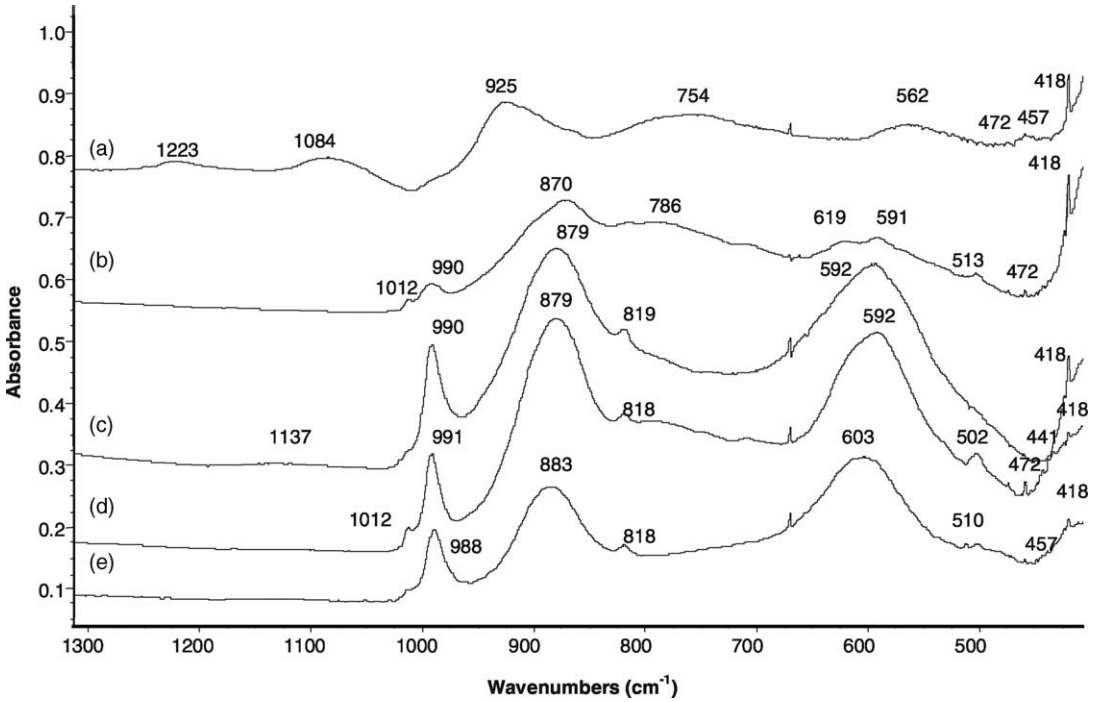


Fig. 4. Room temperature FT-IR spectra of differently calcined samples at 600 °C: (a) nitrogen; (b) static air; (c) dry air; (d) $H_2O$/air; (e) $NH_3$/air.

and 1012 $cm^{-1}$ can be assigned, respectively, to $\nu$(Sb–O–Sb) and $\nu$(V=O···Sb) vibrations of $VSbO_4$ mixed oxide [39]. The broad band at 590–600 $cm^{-1}$ can be assigned to $\nu$(V=O) and the weak band at 510 $cm^{-1}$ to $\nu$(Nb=O) on the basis of data listed for the single oxides in the Atlas of Infrared Spectra of Inorganic Compounds [40]. These data are coherent with the XRD data given above.

In the case of the sample calcined in static air, the intensities of all bands are smaller due to an intense background related to the darker colour of the sample, indicative of a partial catalyst reduction. Nevertheless, the general aspect of the spectrum is similar to those of all air-calcined samples, although a broad band centred near 790 $cm^{-1}$ appeared as for the $H_2O$/air-calcined sample.

For the $N_2$ calcined sample, the IR spectrum is quite different with broad bands at 1223, 1084, 925, 754, 562, and 457 $cm^{-1}$, and an intense background, indicative of a coloured and partially reduced catalyst. To gain additional insight, Sb–Mo mixed oxide with a theoretical elemental composition $Sb_4Mo_{10}O_{31}$ was synthesised and calcined at 500 °C. However, although the Mo/Sb ratio of the sample was found equal to 2.52 by ICP analysis, the XRD pattern corresponds rather to the $Sb_2Mo_{10}O_{31}$ phase, indicating that some amorphous Sb oxide was also formed. The IR spectrum presented broad bands centred at 1088, 918, 472 and 458 $cm^{-1}$. This enabled us to the assign the peaks at 1084, 925, 472 and 457 $cm^{-1}$, observed in Fig. 4a for the $N_2$ calcined sample, to the $Sb_2Mo_{10}O_{31}$ phase. The band at 418 $cm^{-1}$ is also found in some of the spectra of samples calcined in air and can be attributed to $Sb_2O_3$ (sharp peak at 400 $cm^{-1}$). The broad band at 754 $cm^{-1}$ can be assigned to β-$Sb_2O_4$, as observed by Cody et al. for a nitrogen-calcined VSbO catalyst [41], the band at 562 $cm^{-1}$ to $\nu$(V–O–V) vibration in which vanadium is partially reduced and the shoulder at 990 $cm^{-1}$ to $\nu$(Mo=O) in $MoO_3$. The low intensities of these three latter bands indicate that the main phase in this case is the Sb–Mo–O phase, which is in agreement with the XRD results. This infrared study in

complement to the XRD studies indicates that in both cases, one has an intimate mixture of several phases, some of them being XRD amorphous.

The main phase found for the samples calcined in air is $MoO_3$. It is well known since the pioneer work by Kihlborg in the Sixties [42,43], that $MoO_3$ forms oxygen defect shear structures. These sub-oxides of molybdenum have the general formula $Mo_nO_{3n-m}$, where $n = 4, 5, 8, 9$ and $m = 1$ corresponding to the stoichiometries $Mo_4O_{11}$, $Mo_5O_{14}$, $Mo_8O_{23}$, $Mo_9O_{26}$. Other structures, such as $Mo_{17}O_{47}$, $Mo_{18}O_{52}$, etc. also exist. Mestl and co-workers [44,45] prepared some of these sub-oxides with V and W substitutions for Mo and tested them in various oxidation reactions. Based on their results, they concluded that $MoO_3$ is a non-selective catalyst, while V and W substituted $Mo_5O_{14}$ appears to be selective in partial oxidation reactions. Therefore, it is possible to predict that the presence of $MoO_3$ after calcination in oxidative atmosphere will result in less selective reaction, i.e. in higher $CO_x$ formation compared to the catalyst calcined in nitrogen.

The $Mo_5O_{14}$ sub-oxide is a quite interesting material. $Mo_5O_{14}$ (designated as $\theta$-molybdenum oxide) together with $Mo_{17}O_{47}$ (designated as $\chi$-molybdenum oxide) were observed long time ago by Kihlborg in a study of the binary system $MoO_2$–$MoO_3$ [42,43]. The structure of $Mo_5O_{14}$, described by Kihlborg [43], is a complex pattern of metal–oxygen $MoO_6$ octahedral and $MoO_7$ pentagonal bi-pyramids linked by sharing corners and edges, as represented in Fig. 5. The lattice parameters of the tetragonal sub-cell were found equal to $a = b = 22.989$ Å and $c = 3.938$ Å, i.e. u.c. volume of 2081 Å$^3$. Such a phase was observed to be metastable [43,46] and to decompose to a mixture of $Mo_{17}O_{47}$ and $MoO_3$ and further to $MoO_2$ and $MoO_3$, but was shown to be stabilised by a partial substitution of transition metals such as V, Nb and W for Mo [43]. The ternary phase diagram of $(M_xMo_{1-x})_5O_{14}$ with M: V or Nb was established by Ekström and Nygren [46,47]. They found that the pure $\theta$ phase was obtained in the range $x = 0.06$–$0.11$ for V [46] and $x = 0.05$–$0.15$ for Nb [47], and in mixtures for $x$ up to 0.2 for V and up to 0.4 for Nb. The a and b parameters were observed to decrease and the c parameter to increase with increasing V substitution for Mo, resulting in a negligible u.c. volume change, although $V^{5+}$ radius is smaller than $Mo^{6+}$ in six coordination

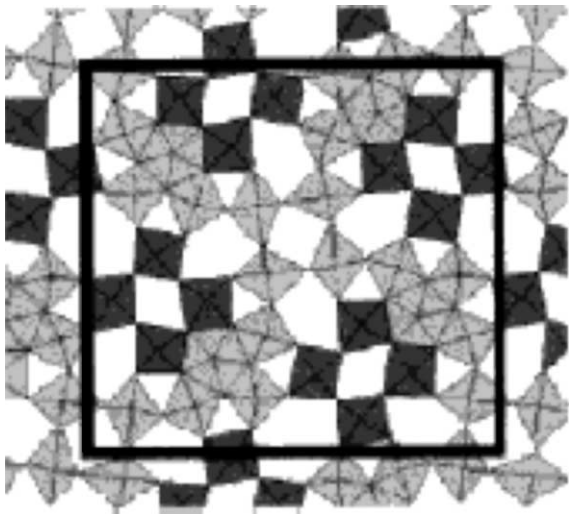

Fig. 5. Crystal structure of $Mo_5O_{14}$ taken from [45].

(0.54 against 0.59 Å). For Nb, the a and b parameters were similar while the c parameter increased with increase in Nb content [47], resulting in a slight increase in the u.c. volume up to 2100–2105 Å$^3$ (radius of $Nb^{5+} = 0.64$ Å in six coordination). In our case, the calculations from XRD patterns gave $a = b = 22.810$ Å and $c = 4.042$ Å, i.e. u.c. volume of 2103 Å$^3$ for air calcined samples and $a = b = 22.898$ Å and $c = 4.025$ Å, i.e. an u.c. volume of 2110 Å$^3$. These data indicate that both Nb and V cations substitute Mo in the $Mo_5O_{14}$ structure.

All catalysts were also characterised by XRD after 4.5 h catalytic testing (Table 1(B); after 4.5 h reaction). Only minor changes were detected for the 500 and 600 °C $N_2$-calcined samples, for which a small transformation of $Sb_2Mo_{10}O_{31}$ to $Sb_4Mo_{10}O_{31}$ was observed, indicating that both phases are certainly present during catalytic reaction. This also supports the concept of the dynamic aspect of the active sites and its role in the deactivation process.

### 3.3. Characterisation of the acidity and of the state of the surface layers of the catalysts

The acidity of the samples was determined by ammonia TPD as summarised in Table 2 after normalisation to the same weight of catalyst. In order to support the TPD results, acid–base titration was

Table 2
Acidity determined by ammonia TPD and titration for 200 mg sample

| Catalyst | $NH_3$–TPD results | | | | $H^+$ titration | |
|---|---|---|---|---|---|---|
| | $NH_3$ mol[a] | $-\log_{10}[NH_3]$[a] | $NH_3$ mol[b] | $-\log_{10}[NH_3]$[b] | $-\log_{10}[NH_4^+]$[a] | $-\log_{10}[NH_4^+]$[b] |
| 600°C/air | $15 \times 10^{-7}$ | 5.8 | $11 \times 10^{-7}$ | 5.9 | 5.5 | 5.4 |
| 600°C/$N_2$ | $1.1 \times 10^{-7}$ | 7 | $0.9 \times 10^{-7}$ | 7.1 | 6.5 | 6.6 |
| 500°C/$N_2$ | $1.8 \times 10^{-7}$ | 6.7 | $1.4 \times 10^{-7}$ | 6.9 | 6.4 | 6.5 |

The superscript alphabets (a,b) represents the values for repeated experiment.

performed with a standardised solution of $NH_4OH$. The results from these titrations are also listed in Table 2. The p$K_a$ values obtained are very comparable to those from TPD experiments.

The results show that all catalysts have low acidity, especially those calcined in nitrogen. Together with literature data they lead to the view that *higher conversion of propane and production of $CO_x$ will be obtained with air-calcined rather than with nitrogen-calcined samples*.

XPS analyses have been performed to determine the elemental composition and the oxidation states of the cations in the top layers of the catalyst after various calcination and activation treatments [5,6]. The experimental data for surface composition are shown in Table 3. They reveal that, with respect to the bulk, the surface is enriched in Sb (by a factor of 3) and depleted in Nb (by a factor of 2) when the catalyst precursor is calcined in air. The bulk and surface composition are nearly identical when the catalyst is calcined in nitrogen. These results further demonstrate that calcination in oxygen favours the diffusion of the Sb cations, very probably as XRD amorphous $SbO_x$ phase at the catalyst surface.

From the binding energy value for each cation, it is possible to determine their oxidation state by comparing the obtained value with literature data, such as those listed in the Handbook of XPS [48]. Table 4 gives the binding energy values determined for each element, after calcinations in either air or nitrogen, and the corresponding oxidation states determined by comparison to selected reference compounds.

Table 3
Surface and bulk chemical composition determined by XPS and atomic absorption (AA)

| Element | Calcination in air | | Calcination in nitrogen | | AA analysis |
|---|---|---|---|---|---|
| | mol% | Atomic ratio[a] | mol% | Atomic ratio[a] | Atomic ratio[a] |
| Mo $3d_{5/2}$ | 13.8 | 1 | 15.0 | 1 | 1 |
| V $2p_{3/2}$ | 4.3 | 0.31 | 4.6 | 0.31 | 0.30 |
| Sb $3d_{3/2}$ | 8.5 | 0.62 | 3.8 | 0.25 | 0.20 |
| Nb $3d_{5/2}$ | 0.5 | 0.04 | 1.5 | 0.1 | 0.09 |
| O 1s | 72.9 | 5.28 | 75.1 | 5.01 | – |

[a] The atomic ratio is normalised to Mo.

All metal cations are in their highest oxidation state, except for the presence of some $V^{4+}$ and traces of $Mo^{5+}$ and $Sb^{3+}$ for the nitrogen-calcined catalysts. The shape of the V$2p_{3/2}$ peak and its shift to a lower binding energy value are indicative of the presence of reduced vanadyl species. Additional information on

Table 4
Oxidation states of cations at the catalyst surface determined by XPS

| Element | Calcination in air | | Calcination in nitrogen | | Reference compounds [48] |
|---|---|---|---|---|---|
| | Binding energy (eV) | Oxidation state | Binding energy (eV) | Oxidation state | Binding energy (eV) |
| Mo $3d_{5/2}$ | 232.2 | 6+, 5+ | 232.3 | 6+, 5+ | $MoO_2$: 229.2; $MoO_3$: 232.3 |
| V $2p_{3/2}$ | 516.6 | 5+, 4+ (transformation) | 516.2 | 5+, 4+ | $V_2O_5$: 516.8; $VOCl_2$: 516.2; $VO_2$: 515.9 |
| Sb $3d_{3/2}$ | 540.1 | 5+ | 539.3 | 3+ | $Sb_2O_3$: 539.4; $Sb_2O_5$: 540.2 |
| Nb $3d_{5/2}$ | 206.6 | 5+ | 206.3 | 5+ | $KNbO_3$: 206.3; $Nb_2O_5$: 207.0 |
| O 1s | 530.3 | 2− | 530.2 | 2− | $WO_3$: 530.2; $Fe_2O_3$: 530.0 |

Table 5
Catalytic results for all samples calcined under different atmospheres and activated in situ before reaction at 500 °C under 20%$O_2$ in He

| Temperature (°C) | Atmosphere | $C_3$ conversion % | Rate of AA formation ($\times 10^{-4}$ mol/h g) | Selectivity (mol% C) | | | | |
|---|---|---|---|---|---|---|---|---|
| | | | | CO | $CO_2$ | $C_3$= | AA | AcA |
| 500 | Dry air | 5.5 | 1.8 | 29 | 7 | 8 | 24 | 29 |
| | $H_2O$/air | 5.1 | 2.0 | 36 | 10 | 9 | 20 | 24 |
| | $NH_3$/air | 6.1 | 3.4 | 33 | 9 | 8 | 22 | 27 |
| | $N_2$($O_2$/He) | 7.5 | 5.9 | 15 | 7 | 11 | 32 | 33 |
| | $N_2$(He) | 11.4 | 14.5 | 10 | 4 | 13 | 54 | 18 |
| 600 | Dry air | 5.4 | 1.2 | 27 | 7 | 7 | 23 | 34 |
| | $H_2O$/air | 3.8 | 1.3 | 34 | 6 | 8 | 19 | 26 |
| | $NH_3$/air | 6.7 | 3.2 | 33 | 6 | 8 | 24 | 27 |
| | $N_2$($O_2$/He) | 1.3 | 1.0 | 10 | 2 | 10 | 32 | 42 |
| | $N_2$(He) | 1.5 | 2.3 | 3 | 2 | 21 | 35 | 35 |
| | Static air | 2.2 | 1.3 | 16 | 2 | 8 | 27 | 43 |

The conditions of activation for nitrogen calcined samples are shown in the brackets.

the Mo(V) and V(IV) species was obtained by ESR and reported earlier [5,6]. They support these XPS observations and assignments.

### 3.4. Effect of various activation treatments on catalytic performance

Catalytic tests were performed with catalysts calcined at 500 and 600 °C in air (wet or dry), $NH_3$/air, and nitrogen, as indicated in Table 5. The samples were further activated at 500 °C in 20%$O_2$ in He unless mentioned otherwise. The observed conversions and selectivities, as well as the rates of formation of AA are also given in Table 5. Fig. 6 plots conversion, BET surface area, and the rate of AA formation as a function of temperature and calcinations/activation treatments, whereas Fig. 7 does the same for the selectivities to $CO_x$, propene ($C_3$=), AA, and AcA.

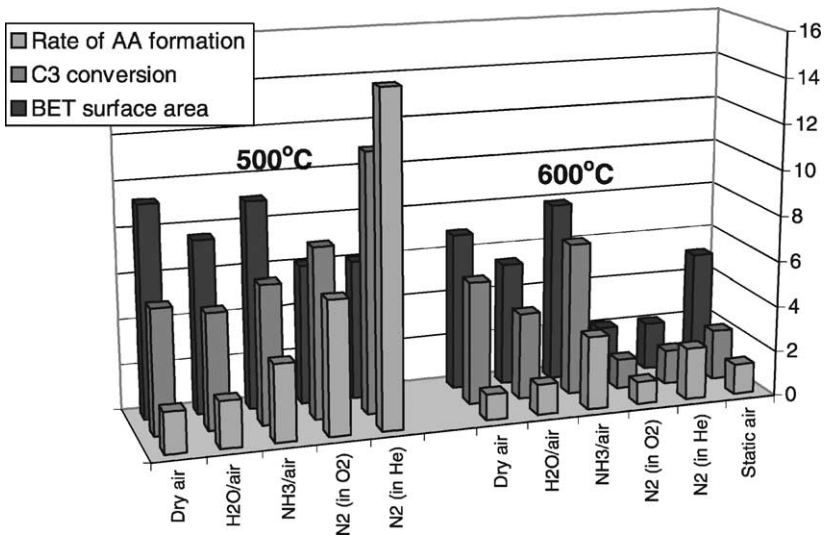


Fig. 6. Comparison between conversion (%), rate of AA formation ($\times 10^{-4}$ mol $h^{-1}$ $g^{-1}$) and $S_{BET}$ ($m^2$ $g^{-1}$) for samples calcined at 500 or 600 °C under the atmosphere indicated and activated at 500 °C under 20% $O_2$ in He, unless stated otherwise in parentheses.

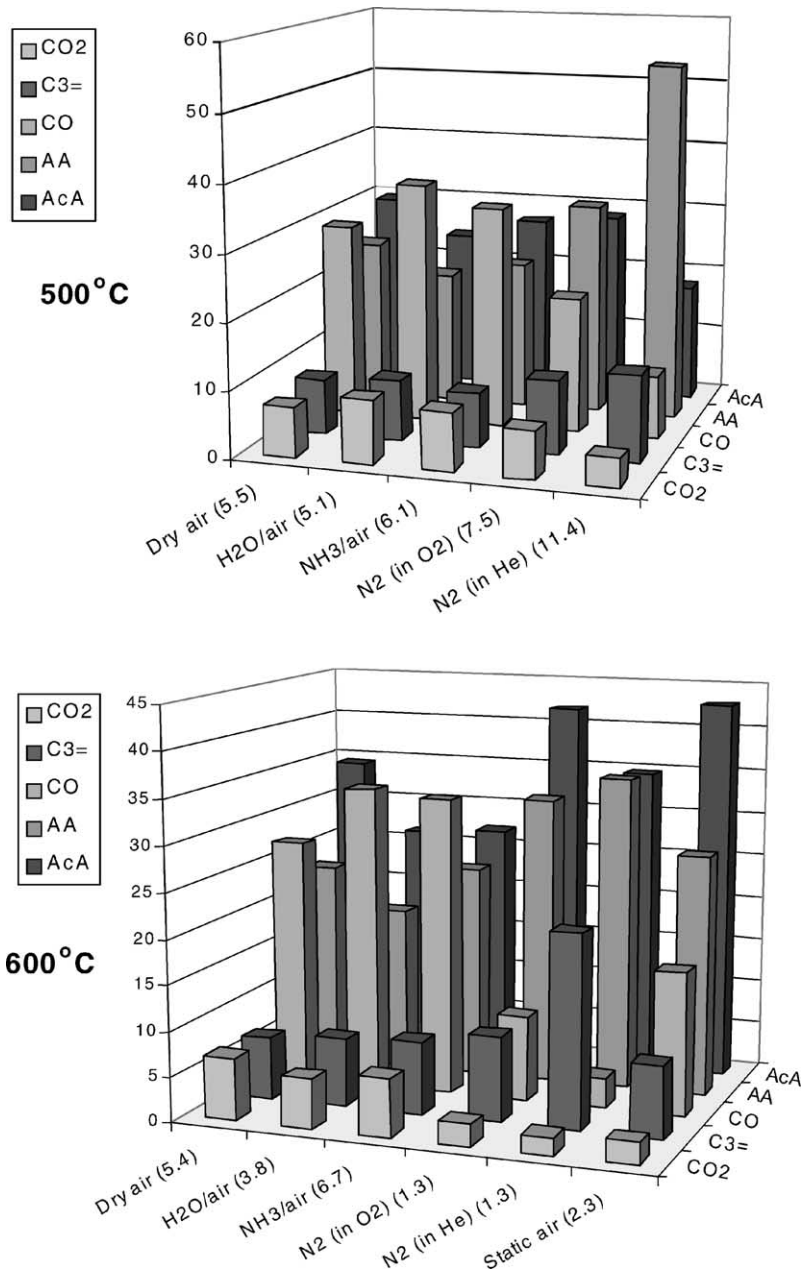


Fig. 7. Products selectivity (mol% C) for various catalysts, calcined at 500 °C (top) and 600 °C (bottom) (propane conversion is added in parentheses next to the calcination atmosphere).

The following observations are made:

1. For air-calcined samples, catalysts calcined at 500 °C give higher propane conversion in parallel to the change in surface area. This does not hold true for $N_2$ calcined samples.
2. Calcination at 500 °C under $N_2$ followed by activation under helium gives the higher propane

conversion and the highest acrylic acid (AA) (54 mol% C at 11.4% propane conversion) and propene selectivities and the lowest $CO_x$ selectivity. It is also remarkable that the selectivity to acrylic acid is higher than that to acetic acid, which is opposite to what was observed for the other catalysts. The selectivity to acetic acid (AcA) is relatively high in all cases at variance with literature data when Te was used instead of Sb, particularly when activation was performed under $O_2$/air.

3. Calcination under static air at 600 °C gives high selectivity to acetic acid, comparable to that observed for the 600 °C $N_2$ calcined sample activated under $O_2$/He.
4. For the air-calcined samples, with and without addition of $NH_3$ or $H_2O$, the major products are $CO_x$, acetic and acrylic acids with average selectivities of about 40, 28 and 22 mol% C, respectively, at 5.4% average ropane conversion.
5. The selectivities to acetic and acrylic acids for the air-calcined catalysts decrease in the order: static air > dry air > $NH_3$/air > $H_2O$/air.
6. The CO selectivity prevails over that of $CO_2$ in all cases by a factor of four for the air-calcined samples, which could indicate that these species originate from different reaction intermediates and products. Some $CO_2$ can be formed together with acetic acid by the oxidation of acetone (the stoichiometry of this reaction is AcA:$CO_2$ = 1:1) and some other from the over-oxidation of the acid products.

Based on these results, one can tentatively propose the reaction network schematised in Fig. 8, where the relative importance of the two major pathways is presumably controlled by the nature of the solid phases at the catalyst surface.

A close look at the catalytic results reveals that the calcination and activation conditions impact not only on the relative rates of formation of the various products, but also one the main pathway by which they are formed. As shown by the XRD, FTIR, and XPS results, the air-calcined samples show the presence of $MoO_3$ as a major phase, which is the probable reason for the higher selectivity to $CO_x$ compared to the catalysts calcined in $N_2$ and in static air. The presence of $Sb_4Mo_{10}O_{31}$/ $Sb_2Mo_{10}O_{31}$ for the $N_2$-calcined samples, $SbVO_4$ for the air-calcined samples, and/or a molybdenum sub-oxide, such as $Mo_8O_{23}$ (traces)

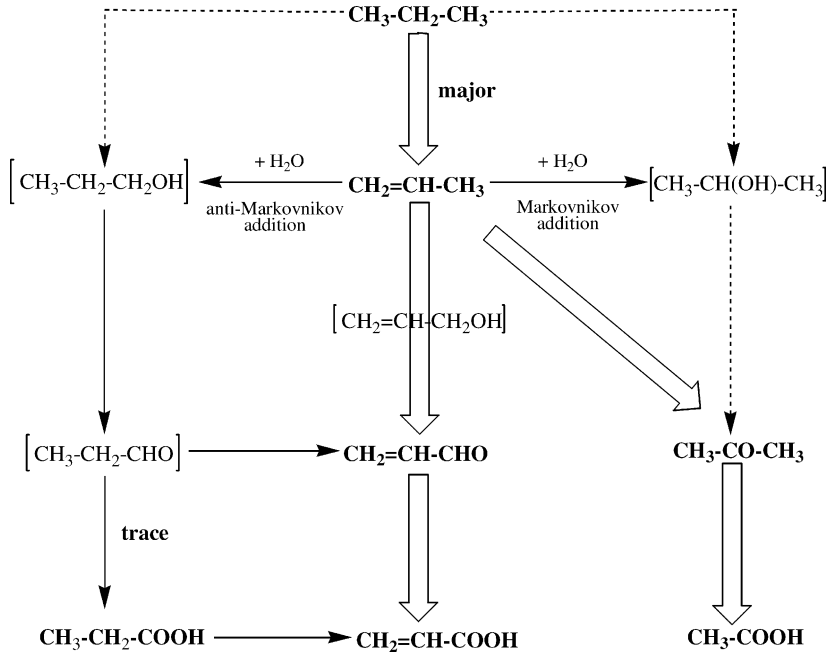


Fig. 8. Mechanism network proposed for propane oxidation on MoNbSbV mixed oxides.

and/or $(M_xMo_{1-x})_5O_{14}$ for all samples appears determining for the formation of the desired acrylic and acetic acid products. This proposal is further supported by the acidity studies described earlier, which suggested that the higher acidity in air-calcined samples (due to the presence of $MoO_3$) should lead to higher activity and, consequently, selectivity to combustion products.

## 4. Discussion and conclusions

The present study shows that the calcination and activation treatments and conditions have a major effect on the structural features and catalytic properties of MoNbSbV mixed oxides. The best conditions for the selective oxidation of propane to acrylic acid comprise calcination under nitrogen at 500 °C and activation in inert atmosphere (He) at 500 °C, followed by calcination under static air. A mixture of several phases, such as $Sb_4Mo_{10}O_{31}/Sb_2Mo_{10}O_{31}$ and a molybdenum sub-oxide such as $Mo_8O_{23}$ and/or $(M_xMo_{1-x})_5O_{14}$ appear to be determining for the selective oxidation of propane.

The $Sb_4Mo_{10}O_{31}/Sb_2Mo_{10}O_{31}$ phases have already been observed in previous studies. They were identified as the phases M1 and M2 by Ushikubo et al. [49]. Their structures were determined by Parmentier et al. for $Sb_4Mo_{10}O_{31}$ [50] and $Sb_2Mo_{10}O_{31}$ [51] and that of $TeMo_5O_{16}$ by Forestier et al. [52]. The structural relation between $Sb_4Mo_{10}O_{31}$ and $Sb_2Mo_{10}O_{31}$ with the $Te[MO_3]_{2n+1}$ phases (with $n = 1$ or 2 for M1 and M2 respectively), was shown by Aouine et al. [53]. They are inter-related structures and are considered as stacking models built up from simple (M1) or double (M2) sheets of $MO_6$ octahedra (M: Mo, V, Nb) separated by row of hexagonal windows forming channels as shown in Fig. 9. The Te or Sb cations occupy the channels formed by the $MO_6$ (M: Mo, V, Nb) octahedra and Sb may also partly occupy the M sites. Consequently, both phases are systematically formed concomitantly and an intergrowth between M1 and M2 structures was even proposed [54]. It is quite possible that, in our case, as for the $Mo_5O_{14}$ phase, some V and Nb cations have partly replaced Mo in the $Sb_4Mo_{10}O_{31}$ and $Sb_2Mo_{10}O_{31}$ phases, resulting in mixed oxides whose formulae are then $Sb_4M_zMo_{10-z}O_{31}$ and $Sb_2M_zMo_{10-z}O_{31}$ with $z$ denoting the small amount of substitution of Mo by M (M: V and/or Nb).

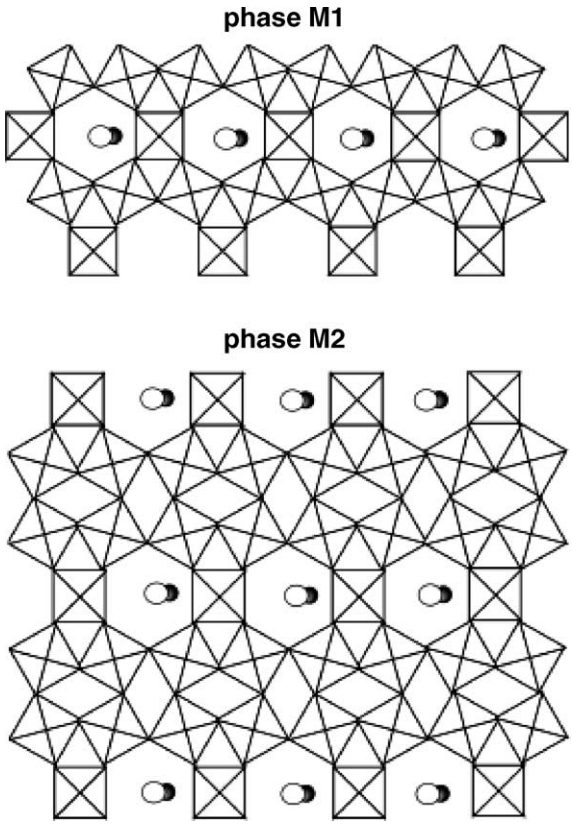


Fig. 9. Representation of the structure of the phases M1 and M2 along the *c*-axis constituted by row of $MO_6$ octahedra. Sb are located in the hexagonal channels (from [53]).

Ushikubo et al. in a study of the propane ammoxidation on MoNbVTe mixed oxides [49] suggested that propane is activated on the M1 phase to give propene, which is then ammoxidised on the M2 phase. Botella et al. found a new MoVTe mixed oxide [55] active for the propene oxidation to acrolein and acrylic acid, which, however, was unable to activate propane. They identified the presence of the M1 phase only and suggested, therefore, that for the MoVTeNb mixed oxide system propane should rather be activated on the M2 phase and then oxidised on the M1 phase. Whichever situation holds, it is clear that both the M1 and M2 phases must be present simultaneously, presumably as an intergrowth, for the catalyst to convert, selectively and with reasonable yield, propane to acrylic and/or

acetic acids. Botella et al. also emphasised that both Nb and Te have to be present to enable the activation of propane and that the presence of several phases, assumed to play a determining role in the reaction, was necessary [55]. Other recent reports support these conclusions, in particular for the MoNbTeV [56] and MoNbSbV mixed oxide systems [57].

With due consideration to the complexity of such systems and of the results themselves, some general trends and conclusions can be drawn from the present study. Propane is activated on one phase, such as $SbVO_4$ and/or $Sb_4M_zMo_{10-z}O_{31}$, to propene which is then oxidised to acrylic and acetic acids on $Sb_2M_zM_{10-z}O_{31}$ (with $z$ referring to V and/or Nb) and/or $(M_xM_yMo_{1-x-y})_5O_{14}$, with x: V and y: Nb. The latter statement is based on the fact that a doped VMo oxide is used industrially for the oxidation of acrolein to acrylic acid at ca. 250 °C [58] and that the presence of the $(M_xMo_{1-x})_5O_{14}$ phase has been identified recently in a mixed Mo–V oxide used for the acrolein oxidation to acrylic acid [59].

It appears that the substitution of Sb for Te, although patented for the propane oxidation to acrylic acid [4], leads to a catalyst that is indeed active for the propane oxidation to acrylic acid, but also yields a relatively high amount of acetic acid via the "acetone pathway" shown in Fig. 8. Thus, this material may not be as promising as expected. It may be that the rates of acrylic and acetic acids formation are related to the $Sb_4M_{10}O_{31}/Sb_2M_{10}O_{31}$ ratio and on the amount of V and Nb substitution for Mo in the $Mo_5O_{14}$ and/or in SbMoO phases.

## Acknowledgements

P. Delichère from the "Institut de Recherches sur la Catalyse", CNRS, Lyon-Villeurbanne, France is thankfully acknowledged for XPS measurements and interpretation.

## References

[1] Mitsubishi Chem. Corp., JP 10045664-A (1996).
[2] Toa Gosei Chem. Ind. Ltd., JP 10137585-A (1996).
[3] M. Lin, M.W. Linsen, EP0962253-A3 (1999) assigned to Rohm and Haas.
[4] M. Takahashi, X. Tu, T. Hirose, M. Ishii, US 5,994,580 (1999) assigned to Toa Gosei.
[5] E. Novakova, PhD thesis, University of Liverpool, UK, February 2002.
[6] E. Novakova, J.C. Védrine, E.G. Derouane, Parts I and II, J. Catal. 211 (2002) 226, Part 1, and 211 (2002) 235, Part 2.
[7] L. Chen, C. Bouchy, J. Tabatabatei, N. Winterton, J.C. Védrine, E.G. Derouane, in: E.G. Derouane et al. (Eds.), Principle and Methods for Accelerated Catalyst Design and Testing, Kluwer Academic Publishers, Dordrecht, 2002, pp. 291–297.
[8] B. Grzybowska-Swierkosz, Top. Catal. 11–12 (2000) 23.
[9] P. Mars, D.W. van Krevelen, Chem. Eng. Sci. Suppl. 3 (1954) 41.
[10] J. Haber, B. Grzybowska, J. Catal. 28 (1973) 489.
[11] B. Grzybowska, J. Haber, J. Janas, J. Catal. 49 (1977) 150.
[12] R.K. Grasselli, J.D. Burrington, Adv. Catal. 30 (1981) 133.
[13] J.C. Védrine, J.-M.M. Millet, J.-C. Volta, Catal. Today 32 (1996) 115.
[14] J.C. Védrine, Stud. Surf. Sci. Catal. 110 (1997) 61.
[15] A. Pantazidis, A. Auroux, J.-M. Herrmann, C. Mirodatos, Catal. Today 32 (1996) 81.
[16] K. Aït-Lachgar, A. Tuel, M. Brun, J.M. Herrmann, J.M. Krafft, J.R. Martin, J.C. Volta, M. Abon, J. Catal. 177 (1998) 224.
[17] J.C. Védrine, Catal. Lett. 2002, in press.
[18] G. Centi, F. Cavani, F. Trifirò, Selective Oxidation by Heterogeneous Catalysis, Kluwer Academic Publishers, New York, 2001.
[19] R.K. Grasselli, D.D. Sureh, K. Knox, J. Catal. 18 (1970) 356.
[20] R.K. Grasselli, D.D. Sureh, J. Catal. 25 (1972) 273.
[21] J.L. Callahan, R.K. Grasselli, AIChE J. 9 (1963) 755.
[22] R.K. Grasselli, J.M. Thomas, The role of site isolation and phase cooperation in selective oxidation catalysis, Top. Catal. 15 (2001).
[23] J. Haber, Stud. Surf. Sci. Catal. 72 (1992) 279.
[24] O. Legendre, Ph. Jaeger, J.P. Brunelle, Stud. Surf. Sci. Catal. 82 (1992) 387.
[25] J.M.M. Millet, H. Ponceblanc, G. Coudurier, J.M. Herrmann, J.C. Védrine, J. Catal. 72 (1992) 387.
[26] L.T. Weng, B. Delmon, Appl. Catal. A: Gen. 81 (1992) 141.
[27] B. Delmon, G.F. Froment, Catal. Rev.-Sci. 39 (1996) 69.
[28] S. Breiter, M. Estenfelder, H.-G. Lintz, A. Tenten, H. Hibst, Appl. Catal. A: Gen. 134 (1996) 81.
[29] A. Bielanski, J. Haber, Oxygen in Catalysis, Marcel Dekker, New York, 1991.
[30] J. Haber, Stud. Surf. Sci. Catal. 110 (1997) 1.
[31] P.L. Gai, Top. Catal. 8 (1999) 173.
[32] J.C. Védrine, Catal. Today 56 (2000) 455.
[33] G.J. Hutchings, J.K. Bartley, J.M. Webster, J.A. López-Sanchez, D.J. Gilbert, C.J. Kiely, A.F. Carley, S.W. Howdle, S. Sajip, S. Caldarelli, C. Rhodes, J.C. Volta, M. Poliakoff, J. Catal. 197 (2001) 232.
[34] M. Ai, J. Catal. 101 (1986) 389.
[35] M. Ai, Catal. Today 13 (1992) 679.
[36] M.M. Bettahar, G. Costentin, L. Savary, J.C. Lavalley, Appl. Catal. A: Gen. 145 (1996) 1.

[37] M. Lin, T.B. Desai, F.W. Kaiser, P.D. Klugherz, Catal. Today 61 (2000) 223.
[38] M.M. Lin, Appl. Catal. A: Gen. 207 (2001) 1.
[39] R. Nilsson, T. Lindblad, A. Andersson, Catal. Lett. 29 (1994) 409.
[40] R. Nyquist, R. Kagel, Infrared Spectra of Inorganic Compounds, Academic Press, New York, 1971.
[41] C.A. Cody, L. Di Carlo, R.K. Darlington, Inorg. Chem. 18 (1979) 1572.
[42] L. Kihlborg, Acta Chem. Scand. 13 (1959) 954.
[43] L. Kihlborg, Acta Chem. Scand. 23 (1969) 1834.
[44] G. Mestl, Ch. Gottschall, R. Linsmeier, M. Dieterle, J. Find, D. Herein, J. Jäger, Y. Uchida, R. Schlögl, J. Mol. Catal. A: Chem. 162 (2000) 455.
[45] M. Dieterle, G. Mestl, J. Jäger, Y. Uchida, H. Hibst, R. Schlögl, J. Mol. Catal. A: Chem. 174 (2001) 169.
[46] T. Ekström, M. Nygren, Acta Chem. Scand. 26 (1972) 1827.
[47] T. Ekström, M. Nygren, Acta Chem. Scand. 26 (1972) 1836.
[48] J.F. Moulder, W.F. Strickle, Handbook of X-ray Photospectroscopy, Perkin-Elmer, USA, 1992.
[49] T. Ushikubo, K. Oshima, A. Kayou, M. Hatano, Stud. Surf. Sci. Catal. 112 (1997) 473.
[50] M. Parmentier, C. Gleitzer, R.J.D. Tilley, J. Solid State Chem. 31 (1980) 305.
[51] M. Parmentier, C. Gleitzer, A. Courtois, J. Protas, Acta Crystallogr. B 35 (1963) 1979.
[52] P. Forestier, M. Goreaud, C.R. Acad. Sci., Paris, Ser. II, (1991) 312.
[53] M. Aouine, J.L. Dubois, J.M.M. Millet, Chem. Commun. (2001) 1180.
[54] S. Vallar, M. Goreaud, J. Solid State Chem. 129 (1997) 303.
[55] P. Botella, J.M. López Nieto, B. Solsona, Catal. Lett. 78 (2002) 383.
[56] P. Botella, J.B. Solsona, A. Martinez-Arias, J.M. López Nieto, Catal. Lett. 74 (2001) 149.
[57] S.A. Holmes, J. Al-Saeedi, V.V. Guliants, P. Boolchand, D. Georgiev, U. Hackler, E. Sobkow, Catal. Today 67 (2000) 403.
[58] R.H. Munch, E.D. Pierron, J. Catal. 3 (1964) 406.
[59] O. Ovsitser, Y. Uchida, G. Mestl, G. Weinberg, A. Blume, R. Schlögl, J. Mol. Catal. A: Chem., 2002, in press.